Localized accumulation of tubulin during semi-open mitosis in the *Caenorhabditis elegans* embryo

Hanako Hayashi[a,b,c,*], Kenji Kimura[b], and Akatsuki Kimura[a,b,c]

[a]Department of Genetics (Sokendai-Mishima), School of Life Science, Graduate University for Advanced Studies (Sokendai), Yata 1111, Mishima, Shizuoka 411-8540, Japan; [b]Cell Architecture Laboratory, Center for Frontier Research, National Institute of Genetics, Yata 1111, Mishima, Shizuoka 411-8540, Japan; [c]Transdiciplinary Research Integration Center, Research Organization of Information and Systems, Tokyo 105-0001, Japan

ABSTRACT **The assembly of microtubules inside the cell is controlled both spatially and temporally. During mitosis, microtubule assembly must be activated locally at the nascent spindle region for mitotic spindle assembly to occur efficiently. In this paper, we report that mitotic spindle components, such as free tubulin subunits, accumulated in the nascent spindle region, independent of spindle formation in the *Caenorhabditis elegans* embryo. This accumulation coincided with nuclear envelope permeabilization, suggesting that permeabilization might trigger the accumulation. When permeabilization was induced earlier by knockdown of lamin, tubulin also accumulated earlier. The boundaries of the region of accumulation coincided with the remnant nuclear envelope, which remains after nuclear envelope breakdown in cells that undergo semi-open mitosis, such as those of *C. elegans*. Ran, a small GTPase protein, was required for tubulin accumulation. Fluorescence recovery after photobleaching analysis revealed that the accumulation was accompanied by an increase in the immobile fraction of free tubulin inside the remnant nuclear envelope. We propose that this newly identified mechanism of accumulation of free tubulin—and probably of other molecules—at the nascent spindle region contributes to efficient assembly of the mitotic spindle in the *C. elegans* embryo.**

Monitoring Editor
Yixian Zheng
Carnegie Institution

Received: Sep 29, 2011
Revised: Feb 28, 2012
Accepted: Mar 1, 2012

INTRODUCTION

Microtubules constitute a major cytoskeleton component in eukaryotic cells; they are critical for cell shape determination, cell migration, and mitosis. Structurally, microtubules are polymers of α- and β-tubulin proteins. During mitosis, microtubule assembly is tightly regulated in an intracellular location-dependent manner. The mitotic spindle, which consists of a dense array of microtubules, is formed around the chromosomes to segregate the sister chromatids to the daughter cells (Alberts *et al.*, 2008). The microtubules are critical for the formation and function of the spindle (Inoue, 1981; Wittmann *et al.*, 2001).

Eukaryotic cells adopt several strategies to facilitate the localized assembly of microtubules during mitosis. Many animal cells undergo open mitosis, wherein nuclear compartmentalization is lost upon nuclear envelope breakdown (NEBD) at prometaphase (Beaudouin *et al.*, 2002; Salina *et al.*, 2002), and cytoplasmic tubulin subunits gain access to the nuclear region. Meanwhile, spindle assembly factors (SAFs) are activated locally near the chromosomes to assemble the mitotic spindle (Gruss *et al.*, 2001; Nachury *et al.*, 2001; Wiese *et al.*, 2001). The small GTPase Ran plays a central role in facilitating spindle formation near the chromosomes (Kalab *et al.*, 1999; Ohba *et al.*, 1999; Wilde and Zheng, 1999; Wilde *et al.*, 2001). Ran is activated to its GTP-bound form (Ran-GTP) by the guanine nucleotide exchange factor RCC1 (RanGEF), which is bound to chromatin throughout the cell cycle (Dasso, 1993; Carazo-Salas *et al.*, 1999,

This article was published online ahead of print in MBoC in Press (http://www.molbiolcell.org/cgi/doi/10.1091/mbc.E11-09-0815) on March 7, 2012.

*Present address: Electron Microscope Laboratory, RIKEN Center for Developmental Biology, 2-2-3, Minatojima-minamimachi, Chuo-ku, Kobe, Hyogo 650-0047, Japan.

Address correspondence to: Akatsuki Kimura (akkimura@lab.nig.ac.jp).

Abbreviations used: CCD, charge-coupled device; CeNEBD, *Caenorhabditis elegans* nuclear envelope breakdown; DNC-1/-2, dynactin complex component 1/2; dsRNA, double-stranded RNA; DYRB-1, dynein light chain roadblock type; ER, endoplasmic reticulum; FRAP, fluorescence recovery after photobleaching; GFP, green fluorescent protein; LIS-1, human lissencephaly gene-related protein; NA, numerical aperture; NEBD, nuclear envelope breakdown; NGM, nematode growth medium; NMY-2, nonmuscle myosin; NPC, nuclear pore complex; NuMA, nuclear mitotic apparatus; PBS, phosphate-buffered saline; PBST, phosphate-buffered saline with 0.1% Tween 20; RNAi, RNA interference; SAF, spindle assembly factor.

2001). Ran-GTP dissociates SAF–importin complexes in order to activate SAFs, such as TPX2 (Gruss *et al.*, 2001) and the nuclear mitotic apparatus (NuMA) protein (Nachury *et al.*, 2001; Wiese *et al.*, 2001). The area of SAF activation is defined by a diffusion gradient of Ran-GTP centered at the chromosome (Kalab *et al.*, 2002, 2006; Kalab and Heald, 2008).

Cells undergoing closed mitosis, such as fungal cells, adopt yet another strategy. In this type of mitosis, the nuclear envelope remains intact throughout the cell cycle. Thus compartmentalization of the nuclear space is maintained. For assembly of the mitotic spindle during the mitotic phase, SAFs are imported into the nuclear space by a phase-specific nuclear transport mechanism. For instance, in *Schizosaccharomyces pombe*, Alp7p/TACC and Alp14p/TOG are imported during the mitotic phase into the nucleus, where they activate the spindle assembly (Sato and Toda, 2007; Sato *et al.*, 2009). Ran also plays a critical role here in defining the region of spindle assembly. Ran can be found in its GTP-bound form inside the nucleus and in its GDP-bound form in the cytoplasm. The distinct forms of Ran on either side of the nuclear membrane define the direction of nuclear import and export (Ohno *et al.*, 1998; Harel *et al.*, 2003). Ectopic change of Ran-GDP to Ran-GTP in the cytoplasm leads to the loss of nuclear compartmentalization, even in *S. pombe* (Arai *et al.*, 2010; Asakawa *et al.*, 2010).

Some organisms adopt intermediate forms of mitosis, called semi-open mitosis, as seen in *Drosophila melanogaster* (Stafstrom and Staehelin, 1984; Kiseleva *et al.*, 2001), *Asterina miniata* (starfish; Terasaki *et al.*, 2001; Lenart *et al.*, 2003), *Aspergillus nidulans* (De Souza *et al.*, 2004), *Ustilago maydis* (Straube *et al.*, 2003, 2005), and *Caenorhabditis elegans* (Lee *et al.*, 2000). In *C. elegans*, the permeability barrier between the nucleus and the cytoplasm is lost during prometaphase, allowing nuclear proteins, such as free histones, to diffuse into the cytoplasm. This process is commonly known in *C. elegans* research as NEBD (Hachet *et al.*, 2007; Portier *et al.*, 2007). In this article, we refer to this process as *C. elegans* nuclear envelope breakdown (CeNEBD) to discriminate it from the complete nuclear envelope disassembly that occurs in cells undergoing open mitosis. At the same time, the components of the nuclear membrane maintain a spherical shape (Lee *et al.*, 2000; Kirkham *et al.*, 2003; Audhya *et al.*, 2007). This structure may correspond to the so-called spindle envelope observed in several species (Stafstrom and Staehelin, 1984; Harel *et al.*, 1989; Zheng, 2010). We hereafter refer to the membranous structure formed even in the absence of spindle formation as the remnant nuclear envelope (Srayko *et al.*, 2005). Some components like lamin and the nuclear pore complex (NPC) are down-regulated after CeNEBD (Lee *et al.*, 2000); other components remain until the late telophase. Compared with open- and closed-mitosis species, little is known about the mechanism underlying the localized assembly of microtubules during semi-open mitosis. Similar to open-mitosis species, chromatin stimulates microtubule assembly in an Aurora A (*air-1*)-dependent manner in *C. elegans* (Toya *et al.*, 2011). Furthermore, microtubules growing from the centrosomes during mitosis are biased toward chromosomes in a Ran (*ran-1*)-dependent manner (Srayko *et al.*, 2005).

The free subunit concentration has profound effects on the dynamics of multi-stranded filaments such as microtubules (Howard, 2001). Importantly, the accumulation of free tubulin in the nascent spindle region can potentially trigger microtubule formation in an all-or-none manner, ultimately exerting a major effect on construction of an appropriate environment for spindle formation. In this study, we describe the localization of free tubulin subunits, which may contribute to the localized assembly of microtubules during the mitotic process in the *C. elegans* embryo.

RESULTS

Free tubulin accumulates in the nascent spindle region of *C. elegans* embryos

To investigate the possible mechanisms underlying the localized assembly of microtubules, we observed the behavior of β-tubulin fused to green fluorescent protein (β-tubulin::GFP) during the first cell cycle of the *C. elegans* embryo. We noticed that prior to the appearance of filamentous tubulin polymers, tubulin appeared to accumulate uniformly in the nascent spindle region at the onset of spindle formation (Figure 1A, left panels). We hypothesized that free tubulin, possibly α/β-tubulin dimers, might accumulate in the nascent spindle region prior to spindle formation. However, it was difficult to clearly distinguish free tubulin from tubulin polymer (microtubule) by observing normal cells.

To better understand the behavior of free tubulin, we treated embryos with nocodazole to prevent the polymerization of tubulin (Strome and Wood, 1983). This treatment also inhibited the attachment of centrosomes (microtubule-organizing centers) to the female pronuclei. Tubulin accumulated in the pronuclear area of nocodazole-treated embryos (Figure 1A, middle panels). Because this pronuclear area of nocodazole-treated embryos corresponds to the nascent spindle region of untreated embryos, we call this area the nascent spindle region throughout this paper, even though the spindle is not formed in nocodazole-treated embryos. This observation suggests that free tubulin accumulates in the nascent spindle region independent of tubulin polymerization.

There remained the possibility that the accumulation of tubulin inside the nascent spindle region was a consequence of nocodazole treatment rather than a physiological process in normal cells. Inhibition of tubulin polymerization by cold treatment in plants (Schwarzerova *et al.*, 2006) or by cold and nocodazole treatment in cultured cells (Akoumianaki *et al.*, 2009) has been reported to cause aberrant accumulation of soluble tubulin inside the nucleus. It is rather improbable that this is the case in *C. elegans* embryos, because accumulation of tubulin in the nascent spindle region does not specifically occur immediately after nocodazole treatment but at a specific time during the mitotic phase (CeNEBD), as examined in detail in the next section.

To further exclude the possibility that the accumulation of tubulin inside the nascent spindle region resulted from inhibition of tubulin polymerization, we knocked down the dynein heavy chain (*dhc-1*) gene by RNA interference (RNAi). In *dhc-1* (RNAi) cells, microtubule polymerization appears normal, but the association between the female pronucleus and centrosomes is inhibited (Gönczy *et al.*, 1999). As a result, filamentous microtubules are reduced to an undetectable level around female-derived chromosomes. The accumulation of tubulin in the female pronuclear region after CeNEBD was detected upon RNAi-mediated knockdown of *dhc-1* (Figure 1A, right panels). This indicated that the accumulation is not due to inhibition of tubulin polymerization and that free tubulin accumulated in the nascent spindle region prior to spindle formation.

The analyses so far used β-tubulin::GFP to examine the localization of tubulin. We investigated whether GFP affects localization and whether intact tubulin (free of GFP) localizes to the nascent spindle region. First, GFP alone did not accumulate in the female pronuclear region at the same stage (Figure 1A), indicating that the accumulation of β-tubulin::GFP in the nascent spindle region is not a consequence of the GFP fusion. Moreover, this result is incongruent with the possibility that the accumulation of β-tubulin::GFP in the region is due to an optical artifact. The cytoplasm of starfish oocytes is filled with yolk platelets. Thus macromolecules diffuse evenly throughout the nuclear and cytoplasmic regions but not

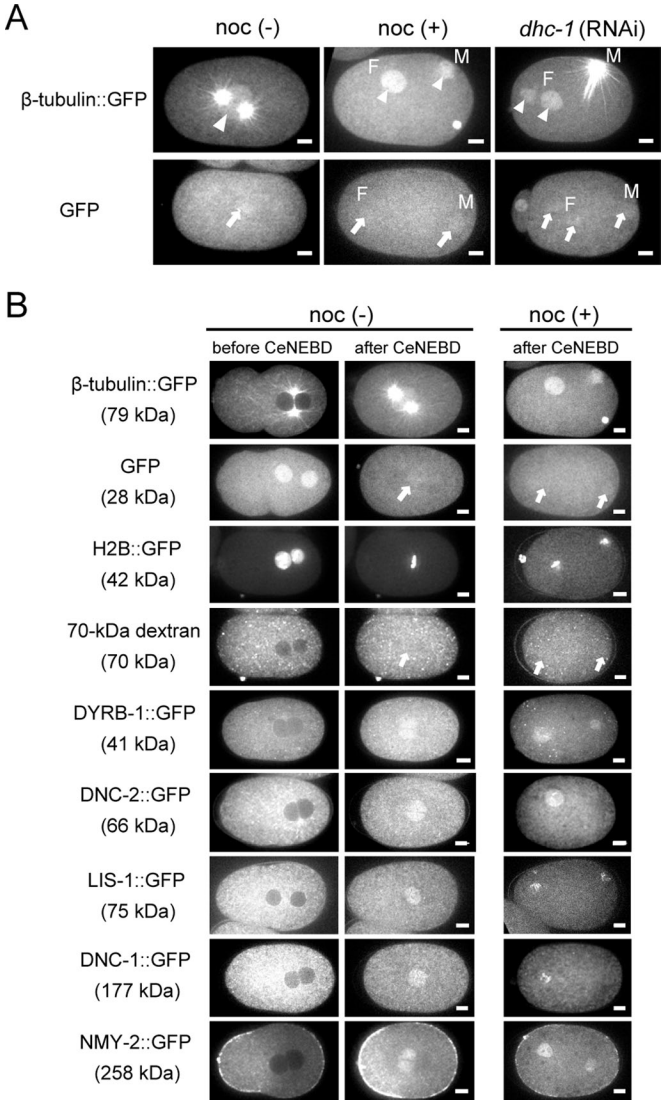

FIGURE 1: Tubulin and other molecules accumulate in the nascent spindle region of the *C. elegans* one-cell-stage embryo. (A) Confocal images of a one-cell-stage embryo expressing β-tubulin::GFP or GFP only, without nocodazole (noc(–)), with 10 μg/ml nocodazole (noc(+)), or treated with *dhc-1* (RNAi). Single optical sections along the equator of the female pronucleus are shown. Arrowheads indicate the accumulation of β-tubulin::GFP. Arrows indicate the position of the pronucleus. M, male pronucleus; F, female pronucleus. Note that aberrant numbers of female pronuclei are observed in *dhc-1* (RNAi) embryos due to a defect in meiosis. (B) Other spindle components accumulate in the nascent spindle region. Confocal imaging of a one-cell-stage embryo without nocodazole (noc(–)) or with 10 μg/ml nocodazole (noc(+)) showing the localization of various macromolecules. Arrows indicate the position of the pronucleus. Scale bars: 5 μm.

within the platelets, and therefore appear to be concentrated in the nuclear region in a nonspecific manner (Lenart *et al.*, 2003). Our observations of GFP localization exclude this effect in the *C. elegans* embryo. Second, we performed antibody staining against intact tubulin in N2 (wild-type) *C. elegans* strain (Supplemental Figure S1) and observed the accumulation of intact tubulin after nocodazole treatment. The nuclear accumulation of tubulin upon knockdown of *dhc-1* has been reported previously (Terasawa *et al.*, 2010). These results collectively support the accumulation of intact tubulin in the nascent spindle region.

Molecules other than tubulin accumulate in the nascent spindle region independent of spindle formation

Previously, human lissencephaly gene-related protein (LIS-1), a regulator of microtubule function, has been shown to localize in the cytoplasm during the interphase and to accumulate in the nascent spindle region during mitosis in the *C. elegans* embryo (Cockell *et al.*, 2004). We also observed similar accumulation of dynactin complex component 1 (DNC-1) and 2 (DNC-2), both of which are subunits of the dynactin complex and are required for spindle formation (Skop and White, 1998; Figure 1B and Supplemental Table S1). Another dynein subunit, dynein light chain roadblock type (DYRB-1), and nonmuscle myosin (NMY-2), also accumulated in the nascent spindle region (Figure 1B and Table S1). The role of DYRB-1 and NMY-2 in the spindle assembly remains unclear, but it has been reported that myosin-1C stabilizes the mitotic spindle in *Dictyostelium discoideum* (Rump *et al.*, 2011). In contrast, neither histone H2B nor 70-kDa dextran accumulated in this region; these results were similar to those seen with GFP alone (Figure 1B and Table S1). DNC-1 and LIS-1 also did not accumulate uniformly in the nascent spindle region after nocodazole treatment (Figure 1B and Table S1). The results indicate that the accumulation is not specific for tubulin nor is it general to all molecules. Importantly, the selective accumulation of these molecules was independent of spindle formation, as we blocked spindle formation by nocodazole treatment. We focused on tubulin to further characterize the nature of this accumulation.

Accumulation starts when permeability across the nuclear envelope rises

The accumulation of tubulin in the nascent spindle region might occur via selective transport across the nuclear membrane before CeNEBD. After CeNEBD, permeability across the nuclear membrane rises, and transport becomes nonspecific. A previous report suggested that accumulation of LIS-1 occurs before CeNEBD (Cockell *et al.*, 2004). In cultured human cells that undergo open mitosis, cyclin B accumulates in the nucleus just before NEBD through a selective import mechanism (Pines and Hunter, 1991; Ookata *et al.*, 1992). We attempted to identify when the accumulation of tubulin takes place in *C. elegans* cells.

To monitor the timing of CeNEBD, we followed the expression of histone H2B::mCherry. Histones are selectively accumulated within the nucleus in interphase, but free histone (which is not incorporated into the chromosome) diffuses throughout the cytoplasm upon CeNEBD (Hachet *et al.*, 2007; Portier *et al.*, 2007). We confirmed that the timing of histone diffusion to the cytoplasm coincided with that of the entry of 70-kDa dextran into the nascent spindle region, which is a general criterion of NEBD (Galy *et al.*, 2003; Lenart *et al.*, 2003; Portier *et al.*, 2007; Figure S2A). The *t* value—calculated by subtracting the mean signal intensity of the cytoplasmic region from that inside the nascent spindle region and dividing the value by the estimated SE—was used to evaluate the statistical significance of the accumulation in the nascent spindle region (Figure 2). On the basis of this value, we determined that histone diffusion into the cytoplasm (i.e., CeNEBD) and tubulin accumulation took place simultaneously in nocodazole-treated embryos. Importantly, in nocodazole-treated embryos, the timing of CeNEBD differs between male and female pronuclei (Hachet *et al.*, 2007; Portier *et al.*, 2007). The timing of tubulin accumulation also differed between male and female pronuclei and coincided with the CeNEBD of each pronucleus. The result indicated that tubulin does not accumulate in the nuclear region before CeNEBD but rather in the nascent spindle region after CeNEBD. We also determined the

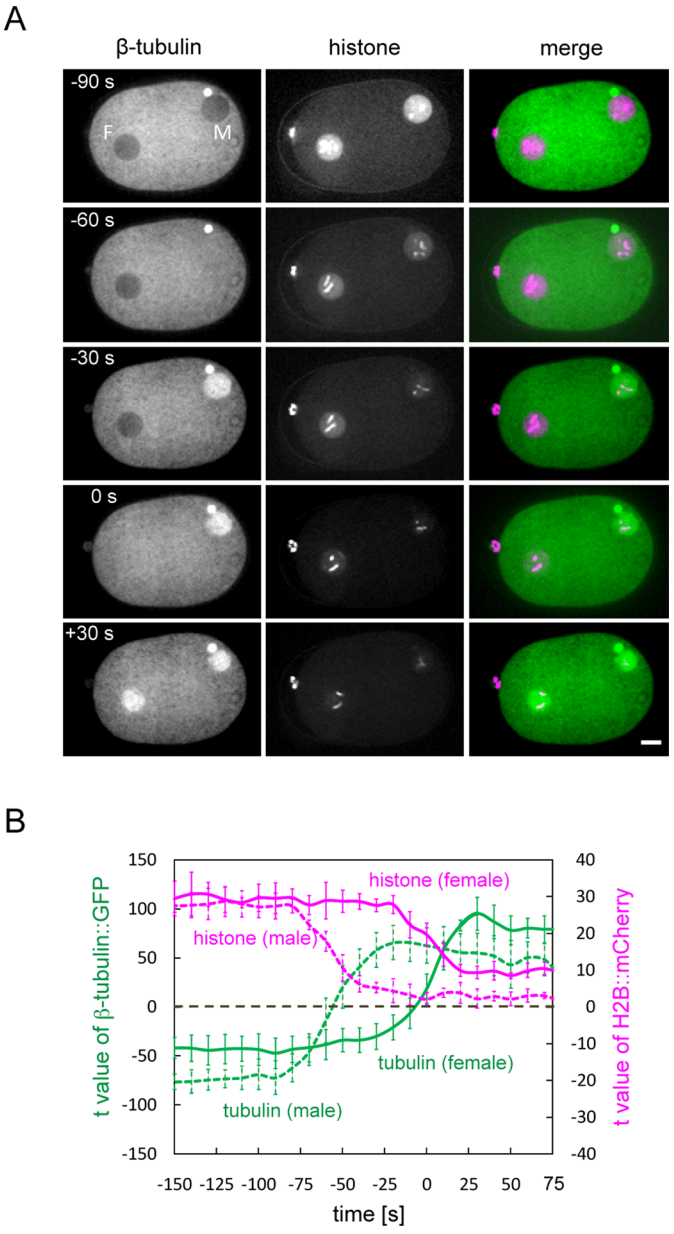

FIGURE 2: Tubulin accumulation occurs during CeNEBD. (A) Confocal time-lapse images of a nocodazole-treated embryo simultaneously expressing β-tubulin::GFP (green) and histone H2B::mCherry (labeling chromosomes and diffusive histones, magenta). The exit of free H2B:mCherry from the pronucleus was used as a marker of CeNEBD. Scale bar: 5 μm. (B) Quantification of the entry kinetics of tubulin (green) and exit kinetics of free H2B::mCherry (magenta) by using *t* values. The *t* value was calculated by subtracting the mean fluorescence intensity of the cytoplasm from that inside the nuclear/nascent spindle region and dividing the difference by the estimated SE. Higher *t* values indicate significant accumulation in the nuclear/nascent spindle region, and negative *t* values indicate brighter intensity in the cytoplasmic region. Note that the CeNEBD of female and male pronuclei takes place at distinct time points in nocodazole-treated embryos (see text). Thus the values were calculated separately for female (solid lines) and male (dotted lines) pronuclei. A "0" indicates the time point of the CeNEBD of a female pronucleus when the *t* value of free H2B::mCherry signals reaches halfway (50%) from the minimum to maximum values for a female pronucleus. The average value ± SD is shown (n = 6).

detailed timing of LIS-1 translocation and found that LIS-1::GFP also translocates after CeNEBD (Figure S2B). This suggests that CeNEBD triggers the nuclear accumulation of tubulin, as well as other molecules. Conversely, it is unlikely that tubulin accumulates via a selective transport mechanism across the nuclear membrane, because the permeability of the membrane increases at CeNEBD. The NPCs responsible for the selective transport are disassembled soon after the CeNEBD (Lee *et al.*, 2000; Galy *et al.*, 2006), whereas the accumulation of tubulin persists. Thus it is unlikely that the accumulation occurs via selective transport.

Untimely permeabilization of the nuclear envelope and the accompanying tubulin accumulation were observed in lamin/*lmn-1* (RNAi)

To obtain insight into the regulatory mechanism of nuclear envelope permeabilization and tubulin influx, we examined the role of lamin/LMN-1. Nuclear lamins form structural layers inside the nucleus and are critical for the integrity of the nuclear envelope (Gruenbaum *et al.*, 2005). LMN-1 is the only nuclear lamin in *C. elegans* (Liu *et al.*, 2000). LMN-1 dissociates from the nuclear envelope after CeNEBD (Lee *et al.*, 2000; Portier *et al.*, 2007), which corresponds to the timing of nuclear envelope permeabilization and tubulin influx. When we knocked down *lmn-1* by RNAi, β-tubulin::GFP was not excluded from the nuclear region at the early stage of the pronuclear migration (Figure 3A). This mislocalization was more evident in nocodazole-treated embryos, which lacked polymerized microtubules (Figure 3B). On the other hand, at the early stage of cortical ruffling (Cowan and Hyman, 2004), we observed exclusion of tubulin from the nuclear region. However, tubulin accumulated in the nuclear region shortly thereafter. This occurred far earlier than in the control embryos. The overall nuclear envelope structure appeared intact under the fluorescence microscope (Figure S3A), although some abnormalities were reported with detailed analysis under an electron microscope (Cohen *et al.*, 2002). The defect in exclusion of the cytoplasmic materials in *lmn-1* (RNAi) was also observed for dextran (Figure S3B). In addition, nuclear materials, such as free histone, diffused into the cytoplasm concurrently with tubulin influx (Figure 3, A and B). Therefore cytoplasmic and nuclear materials were typically mixed when *lmn-1* was knocked down, similar to what we observed after CeNEBD in the normal cells. The dissociation of lamin itself is unlikely be a direct trigger for nuclear envelope breakdown in starfish or vertebrate cells (Beaudouin *et al.*, 2002; Lenart *et al.*, 2003). Combined with these reports, our present result suggests that abolishment of lamin/LMN-1–dependent structures in the nuclear envelope, but not of lamin itself, triggers the permeabilization of the nuclear envelope and the influx of tubulin to the nascent spindle region upon CeNEBD.

Tubulin accumulates inside the "remnant nuclear envelope"

When Srayko *et al.* (2005) found the biased microtubule outgrowth in *C. elegans*, they speculated that the nuclear envelope remaining after CeNEBD (the "remnant nuclear envelope") could be involved in defining the biased region. Because the deformed region of tubulin accumulation appeared to have clear boundaries, we attempted to determine whether these boundaries coincided with the remnant nuclear envelope. When we visualized the remnant nuclear envelope in the SP12 (endoplasmic reticulum [ER]-resident signal peptidase)::mCherry strain (Green *et al.*, 2008), the SP12 signal coincided with the boundary of accumulation (Figure 4, A and B). Therefore the region of the accumulation is probably confined by the remnant nuclear envelope. The remnant nuclear envelope might contribute to biased microtubule outgrowth by blocking

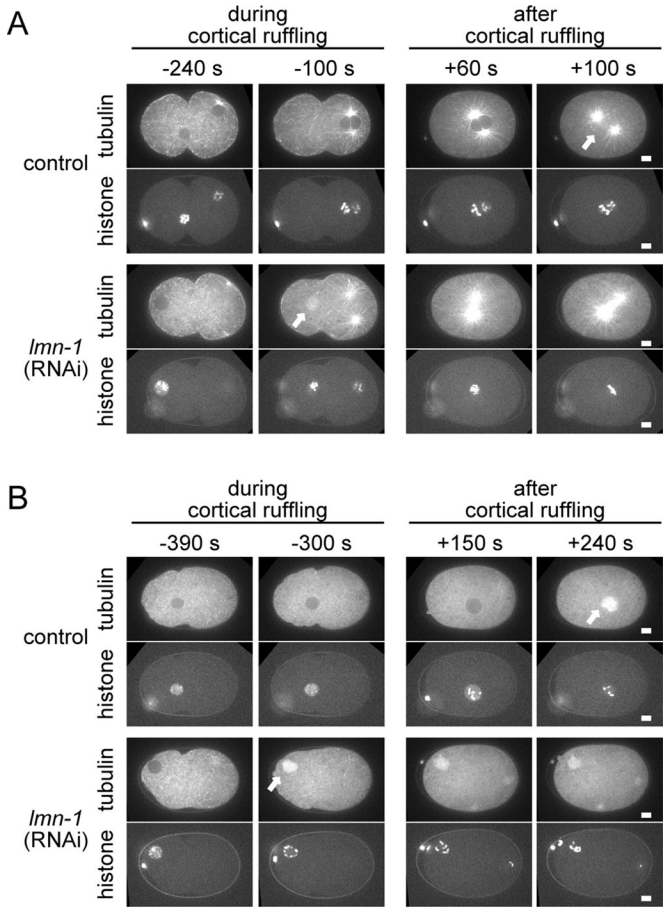

FIGURE 3: *lmn-1* (RNAi) induces untimely permeabilization of nuclear envelope. Time-lapse imaging of wild-type (control) and *lmn-1* (RNAi) embryos expressing β-tubulin::GFP and histone H2B::mCherry without nocodazole treatment (A) or in 10 μg/ml nocodazole (B). Single confocal sections of selected time points during and after cortical ruffling stage after fertilization are shown for each embryo. Time (s) denotes the time elapsed from the completion of cortical ruffling. The accumulation of tubulin (arrows) and diffusion of free histones into cytoplasm is observed after cortical ruffling in control (n = 3/3 for embryos without nocodazole treatment; n = 3/3 for those with treatment), but during cortical ruffling in *lmn-1* (RNAi) (n = 8/8 for those without treatment; n = 10/10 for those with treatment). Scale bars: 5 μm.

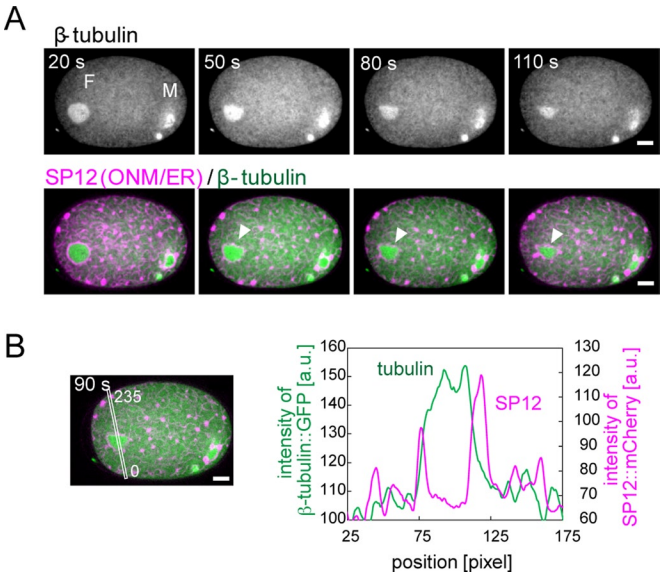

FIGURE 4: The region of tubulin accumulation is delimited by the remnant nuclear envelope. (A) Time-lapse images of β-tubulin::GFP (top) and simultaneous visualization of β-tubulin::GFP (green) and an outer nuclear membrane (OMN)/ER marker (SP12::mCherry; bottom, magenta) in a one-cell-stage embryo treated with nocodazole. Time (s) denotes the time elapsed from the onset of CeNEBD. The white arrowheads denote the deformed tubulin-accumulated region. Scale bars: 5 μm. (B) The overlap of the edge of the tubulin accumulation (green) with the remnant nuclear envelope (magenta). The line-scan graph on the right depicts the position vs. the fluorescence intensity profiles (tubulin, green; SP12, magenta). Scale bars: 5 μm.

microtubule growth across the envelope or actively depolymerizing the microtubule when it reaches the envelope (Srayko *et al.*, 2005). Our results suggests a microtubule polymerization–independent role for the remnant nuclear envelope, in which it functions as a boundary that defines the accumulation of free tubulin. It is unclear at this moment how the permeabilized envelope can function as the accumulation boundary.

Inactivation of Ran inhibits tubulin accumulation in the nascent spindle region

Because biased microtubule outgrowth is dependent on *ran-1* (Srayko *et al.*, 2005), we examined whether the accumulation of free tubulin also depends on *ran-1*. We used RNAi to knock down *ran-1* and examined the localization of tubulin after nocodazole treatment (Figure 5A). During interphase, tubulin was excluded from the nucleus. This exclusion was later lost. However, further accumulation of tubulin in the nascent spindle region was not observed. This result indicates that Ran/RAN-1 is required for tubulin accumulation in the nascent spindle region, which supports localized accumulation of free tubulin being the underlying mechanism for biased microtubule outgrowth in the *C. elegans* embryo.

ran-3, an orthologue of RCC1 (RanGEF) that activates SAFs near chromosomes in cells undergoing open mitosis, was not required for the accumulation of free tubulin in *C. elegans* (Figure 5B). This was not surprising, because *ran-3*, unlike *ran-1*, is dispensable for spindle formation in the *C. elegans* embryo (Askjaer *et al.*, 2002). Although the amino acid sequence of *C. elegans* RAN-3 is similar to that of RCC1 (RanGEF), it is not clear whether *C. elegans* RAN-3 plays an important role, as RCC1 (RanGEF) does in other species. The defective tubulin accumulation in *ran-1* (RNAi), but not in *ran-3* (RNAi), might be the cause of defective spindle formation in *ran-1* (RNAi), but not in *ran-3* (RNAi), embryos.

Because Ran/RAN-1 is a multifunctional protein, we could not specify the mechanism through which Ran/RAN-1 contributed to tubulin accumulation. However, we can exclude some possibilities. We did not observe any apparent defect in the morphological feature of the SP12::mCherry-labeled nuclear envelope in *ran-1* (RNAi) compared with the control or *ran-3* (RNAi) embryos (Figure S4). In addition, the decondensed chromosomes in *ran-1* (RNAi) embryos did not inhibit tubulin accumulation, because the location of the chromosomes did not affect the uniform distribution of tubulin inside the nascent spindle region (Figure S5).

The immobile fraction of tubulin is enriched inside the nascent spindle region in a Ran-dependent manner

So far, we have demonstrated that a specific region around the chromosomes in which tubulin and other molecules accumulate is formed during semi-open mitosis in the *C. elegans* embryo. In closed or open mitosis, the mechanism of formation of such specific

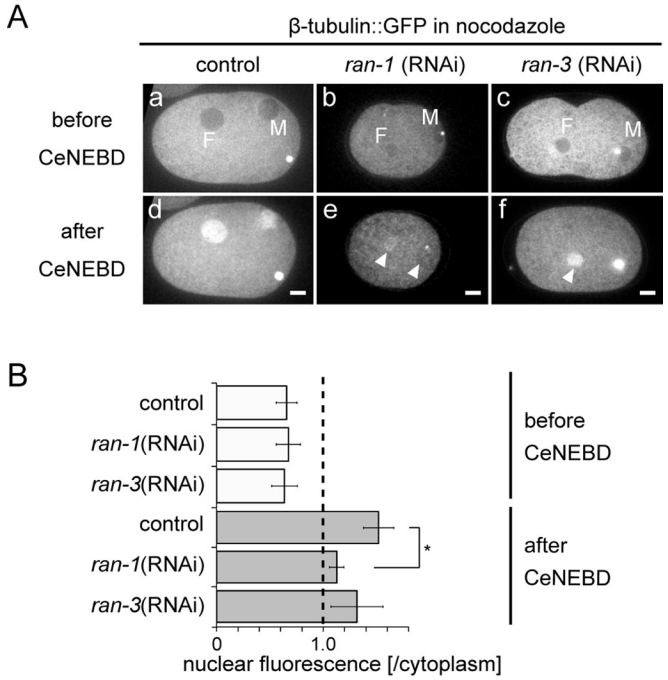

FIGURE 5: Accumulation of tubulin is dependent on *ran-1*. (A) Time-lapse imaging of (a and d) wild-type, (b and e) *ran-1* (RNAi), and (c and f) *ran-3* (RNAi) embryos expressing β-tubulin::GFP in 10 μg/ml nocodazole. Single confocal sections of selected time points before (a, b, and c) and after (d, e, and f) CeNEBD are shown for each embryo. The CeNEBD was determined based on the loss of exclusion of tubulin from the nucleus as an alternative to the exit kinetics of free H2B::mCherry from the nucleus, which was difficult to judge in *ran-1* (RNAi) embryos, because of the impaired chromosome condensation. The arrowhead indicates the location of the pronucleus. Scale bars: 5 μm. (B) Quantification of relative mean β-tubulin::GFP fluorescence intensities in the nuclear/nascent spindle region compared with the cytoplasmic region. The average value ± SD is shown (controls, n = 12; *ran-1* (RNAi), n = 5; *ran-3* (RNAi), n = 4). A relative intensity of 1.0 indicates the same fluorescence intensity in the nuclear/nascent spindle region as in the cytoplasm. *, $p < 0.001$ by Student's *t* test.

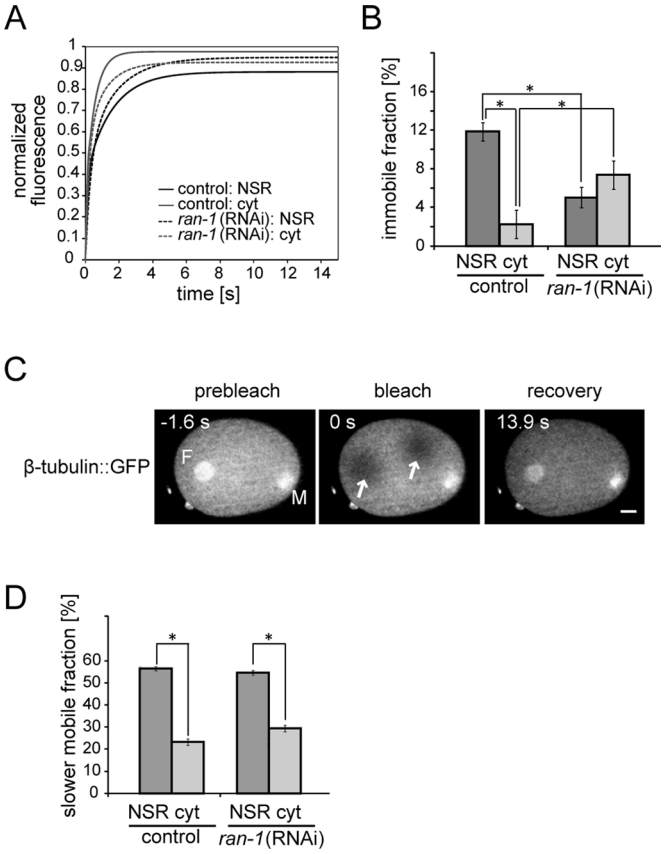

FIGURE 6: Dynamics of tubulin accumulation in the nascent spindle region. (A) The best-fit curves of the normalized fluorescence intensity during the FRAP experiment. Darker gray solid line, nascent spindle region (NSR) of control cells (n = 5); brighter gray solid line, cytoplasmic region (cyt) of control cells (n = 5); darker gray dashed line, nascent spindle region of *ran-1* (RNAi) cells (n = 4); brighter gray dashed line, cytoplasmic region of *ran-1* (RNAi) cells (n = 5). For a raw plot, see Figure S6. (B) The population of immobile fraction (mean% ± [2 × SE]). *, $p < 0.05$. (C) Photobleaching of accumulated β-tubulin::GFP of entire nascent spindle region. A one-cell-stage embryo treated with 10 μg/ml nocodazole was used. Circular regions of 65 pixels in diameter were photobleached simultaneously in both female pronucleus and cytoplasm (arrows) and fluorescence recovery was monitored. The bleached region covers the entire nascent spindle region. Representative images from confocal time-lapse sequences before photobleaching (prebleach), immediately after photobleaching (bleach), and at the time of fluorescence recovery in the bleached region (recovery) are shown. Time (s) denotes the time elapsed from the first acquired frame after bleaching (t = 0 s). Accumulated β-tubulin::GFP signals in the pronucleus completely recovered within 14 s after photobleaching. (D) The population of slower mobile fraction in (A) (mean% ± [2 × SE]). *, $p < 0.05$.

regions around the chromosome involves nuclear compartmentalization by the intact nuclear envelope or a gradient of Ran-GTP (see *Introduction*). However, both scenarios are unlikely in the case of tubulin accumulation in *C. elegans*. The compartmentalization of the nuclear envelope is lost upon CeNEBD, as NPC disassembles (Lee *et al.*, 2000; Franz *et al.*, 2005; Galy *et al.*, 2006), and several macromolecules freely diffuse across the membrane (Figure 1B). It is also thought that the spindle envelope in *Drosophila* does not act as a diffusion barrier (Johansen and Johansen, 2009; Lince-Faria *et al.*, 2009). A simple diffusion gradient of Ran-GTP is also unlikely to be involved in the accumulation, because 1) the shape of the accumulated region is not consistent with a simple gradient (Figure 3) and 2) *ran-3*, a putative counterpart of RCC1 (RanGEF) in *C. elegans*, is not required for the accumulation (Figure 5). A remaining possibility is that the region of tubulin accumulation corresponds to the spindle matrix (Johansen *et al.*, 2011). Ran triggers assembly of the vertebrate spindle matrix (Tsai *et al.*, 2006). Spindle matrix-like structures have been demonstrated in species exhibiting semi-open mitosis, such as *Drosophila* (Lince-Faria *et al.*, 2009) and *A. nidulans* (Ukil *et al.*, 2009).

To obtain insight into the mechanism of tubulin accumulation, we conducted fluorescence recovery after photobleaching (FRAP) analyses (Figure 6). In this technique, a fluorescent molecule in a specific region is photobleached, and the recovery of the fluorescence in the region reflects the mobility of the molecule (Axelrod *et al.*, 1976). We bleached a portion of the nascent spindle region (2 μm in diameter) and quantified the recovery kinetics by using the Olympus FV1000 microscope system (Figure 6, A, B, and D). We compared the recovery kinetics of tubulin between the nascent spindle region and the cytoplasmic (control) region by plotting the normalized fluorescence intensity against the time elapsed and by fitting the plotted points to an exponential curve (Figures 6A and S6). Because the best-fit exponential curve with one exponential component did not give a good representation of the plot, we used

a biexponential curve. A significant difference was detected in the population of the immobile fraction between the nascent spindle region (11.8% ± 1.0% [2× SE]) and the cytoplasmic (control) region (2.3% ± 1.5%; $p < 0.05$; Figure 6, A and B). Importantly, the increase in the immobile fraction in the nascent spindle region, as compared with the cytoplasmic region, was not detected in *ran-1* (RNAi) embryos (nascent spindle region, 5.0% ± 1.1%; cytoplasmic region, 7.4% ± 1.5%; Figure 6, A and B). In the *ran-1* (RNAi) embryos, we observed not only a decrease of the immobile fraction in the nascent spindle region compared with the controls but also an increase of the fraction in the cytoplasmic region. A possible explanation for this observation is as follows: in the wild-type condition, a structure that stably traps tubulin is located only in the nascent spindle region. On *ran-1* (RNAi), the compartmentalization between the nascent spindle region and the cytoplasmic region is lost, and the structure that traps tubulin is diffused to the cytoplasm. Such a scenario can explain the decreased immobile tubulin fraction at the nascent spindle region and, simultaneously, an increased immobile tubulin fraction at the cytoplasmic region.

The mobile fraction of tubulin also contributes to tubulin accumulation

Enrichment of the immobile fraction of tubulin may not be the sole mechanism responsible for tubulin accumulation inside the nascent spindle region. In contrast to the experiment in the preceding section, in which we bleached a portion of the nascent spindle region, we photobleached the entire nascent spindle region after tubulin accumulation in the nocodazole-treated cells by using the Mosaic digital illumination system (Andor Technology). We found that the fluorescence recovered to a level higher than that of the nonbleached cytoplasmic region (Figures 6C and S7). This reaccumulation occurred within ~15 s. On the basis of the previous FRAP analysis after bleaching of a small region (Figure 6A), we concluded that the detected immobile fraction is immobile for >15 s. Thus it is difficult to explain this reaccumulation of the fluorescence based on the contribution of the immobile fraction only. Therefore, in addition to the immobile fraction, a mobile tubulin fraction diffusing in and out of the nascent spindle region might contribute to the accumulation. In this case, we suspect that the mobility of tubulin differs between the nascent spindle region and the cytoplasm.

To explain tubulin accumulation independent of the immobile tubulin fraction, we hypothesized a transient trap (shorter than 15 s) of tubulin in the nascent spindle region. Such a transient trap explains the accumulation and reaccumulation of the fluorescent tubulin to the nascent spindle region within 15 s after photobleaching. The existence of such a transient trap should be reflected in the mobility observed in the FRAP analysis, in which we bleached a portion of the nascent spindle region, because the transient trap should reduce the apparent mobility of the population (Sprague *et al.*, 2004). The $t_{1/2}$ (half-life time) value, which is the time required for the fluorescence of the bleached region to recover half of its plateau intensity, is often used as an index of molecule mobility in FRAP analysis (Axelrod *et al.*, 1976; Sprague *et al.*, 2004). When we fitted the dynamics of the FRAP of a small region in a nascent spindle region and a control region into the biexponential curve model (see *Materials and Methods*), the proportion of the slower mobile fraction ($t_{1/2} = 1.03$ s) against the faster mobile fraction ($t_{1/2} = 0.125$ s) was significantly larger in the nascent spindle region (57% ± 1.0% [2× SE]) than in the control cytoplasmic region (23% ± 1.5%; $p < 0.05$; Figure 6, A and D). The result was consistent with the idea that more tubulin molecules are trapped transiently inside the nascent spindle region, as compared with the cytoplasmic region. However, this increase did not depend on RAN-1, as tubulin in the nascent spindle of *ran-1* (RNAi) embryos had a slower mobile fraction similar to that seen in normal embryos (55% ± 1.1%; Figure 6, A and D). This result indicates that the increase in the slower mobile fraction is independent of *ran-1* and thus cannot account for the *ran-1*–dependent tubulin accumulation. However, we did observe a slight accumulation of tubulin even in *ran-1* (RNAi) embryos (Figure 5), which suggests that a *ran-1*–independent mechanism of tubulin accumulation exists. In conclusion, we propose that an increase in the immobile (for >15 s) and slow-mobile ($t_{1/2}$ is ~1 s) fractions in the nascent spindle region act in concert to favor the accumulation of tubulin in the nascent spindle region.

DISCUSSION

Tubulin accumulates in the nascent spindle region

In this study, we demonstrated that free tubulin accumulates in the nascent spindle region during semi-open mitosis in the *C. elegans* embryo (Figure 1). Because microtubule nucleation and polymerization can be facilitated by an increase in substrate (i.e., free tubulin) concentration, the accumulation of free tubulin may be a mechanism to facilitate microtubule formation in this region. Furthermore, because microtubules are a major component of the mitotic spindle, and the timing and region of accumulation coincides with that of the spindle assembly, we propose that the accumulation of tubulin is a mechanism that facilitates spindle assembly. The phenotype of *ran-1*/Ran (RNAi) embryos supports this notion because RNAi impairs both tubulin accumulation (Figure 5) and spindle formation (Askjaer *et al.*, 2002; Bamba *et al.*, 2002). Importantly, during spindle assembly in the *C. elegans* embryo, it has been reported that microtubule outgrowth is biased at the spindle region in a *ran-1*–dependent manner (Srayko *et al.*, 2005). Our findings further provide a possible explanation for the biased outgrowth of the microtubule, because the localized tubulin accumulation should promote polymerization of the microtubule at this region.

Tubulin may also accumulate in other semi-open mitosis species such as *A. nidulans*. In *A. nidulans*, the nuclear envelope looks intact, but the NPC is partially disassembled during the mitotic phase to allow the entry of cytoplasmic molecules, such as tubulin, into the nuclear space (De Souza *et al.*, 2004). Previous studies clearly showed that tubulin enters the nuclear region in *A. nidulans* (De Souza *et al.*, 2004), but whether the tubulin accumulates at this region to a greater extent than in the cytoplasmic region, as observed in *C. elegans*, is not known (Ovechkina *et al.*, 2003).

Other molecules also accumulate in the nascent spindle region

Molecules other than tubulin accumulate inside the nascent spindle region. Such molecules include dynein-associated protein (LIS-1; Cockell *et al.*, 2004), subunits of the dynein/dynactin motor complex (DNC-1, DNC-2, and DYRB-1), and myosin (NMY-2; Figure 1B). Interestingly, accumulation of DNC-1 and LIS-1 in the nascent spindle region was abrogated by nocodazole treatment, suggesting that association of these molecules with microtubule-based structures drives their localization (Figure 1B). Previous studies reported that LIS-1::GFP (Cockell *et al.*, 2004), Nup107, and MEL-28 (Franz *et al.*, 2005; Galy *et al.*, 2006) accumulate in similar regions during the mitotic phase in the *C. elegans* embryo. However, the precise timing of the accumulation or its dependency on spindle formation had not been clarified for these molecules. Recently, Toya *et al.* (2011) reported that Aurora A/AIR-1 accumulates in a region corresponding to the nascent spindle region prior to tubulin accumulation in the *C. elegans* embryo (Toya *et al.*, 2011). This suggests a

regulatory cascade for the accumulation of various molecules in the nascent spindle region, in which the accumulation of one molecule triggers that of another. Although the accumulation does not occur for all molecules, a variety of molecules may accumulate in the nascent spindle region. On the basis of the features of the accumulated molecules, we consider their accumulation a mechanism that changes the molecular composition around the chromosome to facilitate spindle formation in the *C. elegans* embryo.

Timing of tubulin influx, nuclear envelope breakdown, and lamin function

We demonstrated that the timing of tubulin influx into the nuclear region coincides with the general permeabilization of the nuclear envelope (CeNEBD; Figure 2). In addition, we showed that lamin/LMN-1 is required to prevent the influx of tubulin and other cytoplasmic materials (Figures 3 and S3). The loss of exclusion of tubulin from the nuclear space upon knockdown of lamin-related proteins (emerin/EMR-1 and Lem2/LEM-2) has been previously observed (Meyerzon *et al.*, 2009). However, to our knowledge, it has not been taken into consideration even in this study or in studies involving other model organisms. Untimely permeabilization of the nuclear envelope is an important phenotype resulting from lamin dysfunction and may be implicated in laminopathies, a group of human diseases caused by mutations in lamins and lamin-related molecules (Gruenbaum *et al.*, 2005). Untimely permeabilization of the nuclear envelope and the resulting tubulin accumulation in *lmn-1* (RNAi) also provides better information on the mechanism and the function of tubulin accumulation. A hypothetical substrate to trap tubulin to the nascent spindle region may exist inside the nucleus before CeNEBD or may be formed prematurely inside the nucleus when *lmn-1* is knocked down. The accumulation of tubulin alone is not enough to form the mitotic spindle; we did not observe an apparent untimely spindle in the *lmn-1* (RNAi) embryos.

Role and structure of the remnant nuclear envelope/spindle envelope

Several species, including *C. elegans*, retain the structure of the nuclear envelope after the permeability of the envelope increases (Galy *et al.*, 2003; Lenart *et al.*, 2003; Portier *et al.*, 2007). The role of the remnant nuclear envelope or "spindle envelope" has been unclear. Previous theoretical studies proposed that the membrane components would provide physical strength to the spindle during open mitosis (Civelekoglu-Scholey *et al.*, 2010; Poirier *et al.*, 2010). In this study, we found that the remnant nuclear envelope forms the border of the region in which tubulin accumulates (Figure 4). Nevertheless, the precise role of the envelope for tubulin accumulation is still unclear. Our FRAP experiment, in which we bleached a portion of the nascent spindle region, demonstrates that tubulin is less mobile in the nascent spindle than in the cytoplasmic region, and thus suggests the existence of a hypothetical substrate that traps tubulin. The remnant nuclear envelope may define the limit of the region to which this hypothetical substrate extends, rather than functioning as a diffusion barrier that confines tubulin. For better understanding of the structure and function of the remnant nuclear envelope, detailed characterization of the membrane using electron microscopy (Kirkham *et al.*, 2003) and analysis of the membrane's molecular composition is required.

We also demonstrated that the maintenance of the spherical shape of the envelope requires spindle formation (Figure 4). Under normal conditions, that is, without nocodazole treatment, the remnant nuclear envelope does not deform, but instead exhibits an organized spindle shape (Stafstrom and Staehelin, 1984; Harel *et al.*, 1989; Zheng, 2010). Thus it is suspected that the mitotic spindle provides the framework for the remnant nuclear envelope. Lamin, a component of a subjacent structural layer of the nuclear envelope, disassembles soon after CeNEBD (Lee *et al.*, 2000). This disassembly of lamin and the failure of the microtubule to form the spindle might be the cause of the deformation of the remnant nuclear envelope in nocodazole-treated cells. The mode of interaction between the membrane and spindle components is also an interesting aspect to be studied in the future.

Mechanism of localized tubulin accumulation

We propose that the mechanism of tubulin accumulation is likely to be different from the known mechanisms responsible for the concentration of molecules around the chromosome, such as the Ran-GTP gradient and selective nuclear import. However, the nature of the mechanism of tubulin accumulation in *C. elegans* has not been fully unraveled yet. In this study, we showed that 1) the boundary of the region of accumulation coincides with the remnant nuclear envelope, 2) tubulin accumulation requires *ran-1*/Ran, and 3) tubulin accumulation is accompanied by an increase in the immobile tubulin fraction at the nascent spindle region. On the basis of these observations, we propose the following scenario as a mechanism of localized tubulin accumulation: Before CeNEBD, free tubulins and other materials of the mitotic spindle are excluded from the nucleus to prevent contact with the chromosomes, which might trigger untimely spindle formation. On CeNEBD, the nuclear envelope is permeabilized and free tubulins and other molecules passively diffuse into the nuclear space (i.e., the nascent spindle region). These molecules are trapped in the region bordered by the remnant nuclear envelope and thus accumulate. A structure similar to the spindle matrix in vertebrates may be formed in the same region to trap free tubulins. Considering that *ran-1*/Ran has multiple functions inside the cell, including nuclear import, nuclear envelope assembly, and microtubule stabilization (Askjaer *et al.*, 2002; Salus *et al.*, 2002), it is unclear which of Ran's functions is involved in the accumulation of tubulin. In future experiments, it would be of interest to search for genes specifically involved in tubulin accumulation to gain insight into the mechanism of tubulin accumulation. *C. elegans* counterparts of SAFs enriched in the vertebrate spindle matrix, such as NuMA, Eg5, XMAP215, and poly(ADP-ribose) (PAR; Zheng, 2010), and *Drosophila* microtubule-independent spindle matrix structural proteins, such as Skeletor and Megator (Walker *et al.*, 2000; Qi *et al.*, 2004; Johansen *et al.*, 2011), are promising candidates for study. On another note, and because the accumulation of free tubulin occurs in the vicinity of the chromosomes, the accumulation may also be important for chromatin-stimulated microtubule formation (Toya *et al.*, 2011). Understanding the unique strategy contributing to the change in the molecular environment around the chromosome during semi-open mitosis in *C. elegans* will contribute to better understanding of the common mechanisms underlying various forms of mitosis in eukaryotic cells.

MATERIALS AND METHODS

C. elegans strains and maintenance

The strains used in this study are listed in Table S2. CAL0461 (H2B:mCherry) was obtained by backcrossing OD139 with N2. CAL0451 and CAL0491 were obtained by mating AZ244 with SP12::mCherry or CAL0461, respectively. All *C. elegans* strains were cultured on nematode growth medium (NGM) plates and fed with OP50 *Escherichia coli* according to standard methods (Brenner, 1974). For nocodazole treatment, nocodazole (Sigma-Aldrich, St. Louis, MO) was added to M9 buffer at a concentration of 10 μg/ml

just before observation or fixation, as previously described (Kimura and Onami, 2005; Portier *et al.*, 2007).

Antibody staining

N2 worms were dissected directly on 2% poly-L-lysine-coated glass slides in M9 with or without 10 μg/ml nocodazole. Nocodazole-treated worms were placed at room temperature for 20 min in order to obtain cells undergoing CeNEBD after microtubule depolymerization. The samples were incubated on dry ice for 30 min, after which the eggshell was permeabilized by freeze-cracking, and the sample was fixed in methanol for 30 min at −20°C. The sample was then rehydrated in phosphate-buffered saline (PBS) with 0.1% Tween 20 (PBST) for 30 min. The fixed embryos were incubated with a 1:200 dilution of a mouse monoclonal anti–α-tubulin antibody (DM1A; Sigma-Aldrich). After incubation for 45 min in a humidity box, the embryos were washed twice for 5 min each time in PBST. Secondary antibodies conjugated with Alexa Fluor 488 (Molecular Probes, Eugene, OR) were used at a 1:500 dilution in PBS, incubated in a dark humidity box, and washed twice for 5 min each in PBST. DNA was stained by incubating the embryos for 5 min with 0.02 μg/ml 4′,6-diamidino-2-phenylindole (Sigma-Aldrich) in PBS. Slides were mounted with Slowfade (Molecular Probes) to prevent quenching. Finally, the embryos were sealed with Vaseline. The stained embryos were observed with an Olympus FV1000 confocal fluorescence microscope equipped with a PlanApo 60×/1.4 numerical aperture (NA) lens (Olympus Optical, Tokyo, Japan). Confocal sections along the *z*-axis were obtained at 1-μm intervals. Three-dimensional reconstruction and image processing were carried out with Image J version 1.39e (National Institutes of Health [NIH], Bethesda, MD) and FV1000-ASW software (Olympus).

Live-cell imaging

Adult worms were mounted in M9 with or without 10 μg/ml nocodazole and directly dissected on an 8-well slide. The embryos were sorted with the help of an eyelash brush. A mouth pipette was used to transfer each embryo onto a 2% agar pad mounted on a microscope slide, after which it was covered with an 18 × 18 coverslip (Matsunami Glass Ind., Osaka, Japan). The coverslip was sealed with VALAP (2:2:1 mixture of Vaseline, lanolin, and paraffin) to prevent the embryo from drying. Visualization of GFP or mCherry fusion proteins or Texas Red–labeled dextran was performed by using a spinning-disk confocal system (CSU-X1; Yokogawa Electric, Tokyo, Japan) mounted on a microscope (BX71; Olympus) equipped with an UPlanSApo 100×/1.40 NA objective (Olympus) at room temperature. Images were acquired every 10 s at 100- to 500-ms exposure times. Digital images were obtained by using a charge-coupled device (CCD) camera (iXon; Andor Technology, Belfast, United Kingdom), controlled by MetaMorph imaging software (Molecular Devices, Sunnyvale, CA).

RNAi

RNAi-mediated gene knockdown was performed by injecting double-stranded RNA (dsRNA) into the gonads or the intestine of *C. elegans* larvae (Fire *et al.*, 1998). First, PCR amplification was performed using the *C. elegans* N2 genomic DNA as a template to obtain DNA corresponding to the genes of interest. The sequences of the primers used for PCR amplification are listed in Table S3. For synthesis of dsRNA, in vitro transcription employing T7/T3 polymerase (Promega Corporation, Madison, WI) was done using the PCR products as templates. dsRNA was purified by phenol/chloroform extraction and resuspended in TE buffer. The expected molecular sizes of the purified dsRNAs were confirmed by agarose gel electrophoresis assay. The dsRNA solution was injected into the gonads or the intestine of L4 larvae, and the injected worms were incubated at 22°C for 16–20 h. After this incubation period, the injected worms were individually transferred to new plates and incubated at 22°C for several hours to lay eggs. This was done to test the hatching ratio. The embryonic lethality phenotype of RNAi-injected larvae was evaluated by the ratio of hatching after incubating the plates with eggs at 22°C for another 24 h.

Injection of fluorescently labeled dextran

Injection of dextran was performed as previously described (Galy *et al.*, 2003; Portier *et al.*, 2007). In brief, Texas Red–labeled 70-kDa dextran (emission/excitation = 595/615 nm; Molecular Probes) was diluted to a final concentration of 2 mg/ml in injection buffer (20 mM KPO_4, pH 7.5, 3 mM potassium citrate, pH 7.5, and 2% polyethylene glycol-6000 [Wako Pure Chemical Industries, Osaka, Japan]). The solution was injected into the gonads of young adult worms following the procedure used for injection of dsRNA for RNAi. Injected worms were incubated for 4–5 h at 22°C on NGM plates before observation of the embryos in order to allow incorporation of the dextran into the newly formed embryos.

Image quantification

All image processing and quantification, except for FRAP analysis, were carried out with Image J version 1.39e software (NIH). Normalization and conversion of the measured fluorescence intensity were performed using Microsoft Excel (Microsoft, Redmond, WA).

To quantify the temporal kinetics of tubulin accumulation and free H2B exit (Figure 2), we calculated the *t* value of the fluorescence intensity of the nuclear/nascent spindle region and the cytoplasm. To calculate the *t* values, we quantified the mean and variance of fluorescence intensity of β-tubulin::GFP and free H2B::mCherry within a circular region with the diameter of 36 (β-tubulin::GFP) or 10 pixels (H2B::mCherry). The measurement was conducted for both nuclear/nascent spindle and cytoplasmic regions. The mean fluorescence intensity of the cytoplasmic region was subtracted from the mean fluorescence intensity inside the nuclear/nascent spindle region and divided by the estimated SE to calculate the *t* value. A larger *t* value indicates greater tubulin accumulation. We calculated the signal ratio between nuclear/nascent spindle region and cytoplasm as another index to evaluate the accumulation of β-tubulin::GFP. To calculate the ratio, we quantified the mean fluorescence intensity in the nuclear/nascent spindle region and cytoplasm, as was done for the *t* value calculation. These mean intensities were then normalized by subtracting the mean intensity of a background region (outside the cell), and the ratio was calculated by dividing the mean intensity in the nuclear/nascent spindle region by that in the cytoplasmic region.

For line-scan analysis (Figure 4), the average fluorescence intensity across the nascent spindle region and cytoplasm was measured along the 5-pixel-wide line. A rim of spindle envelope was identified as the peak of SP12::mCherry intensity. The region of tubulin accumulation was determined as the area with the highest intensity (as compared with the intensity in the cytoplasm).

FRAP

To analyze the dynamics of tubulin inside the remnant nuclear envelope, we performed FRAP experiments after tubulin accumulation in nocodazole-treated one-cell-stage embryos. Photobleaching, image acquisition, and image analysis were performed on an Olympus FV-1000 system equipped with a 60×/1.45 NA oil immersion UPlanSApo objective (Olympus) at room temperature. The

imaged region was magnified using electronic optical zooming (5×). Image acquisition was conducted for regions with 256 × 110 pixels (0.099 μm/pixel) at the minimum interval (69 ms) using 488-nm argon lasers at 10% of their power with the pinhole diameter set at 255 μm. Prior to the bleaching, 40 frames of images were acquired. Photobleaching was performed for a circle region of 20 pixels in diameter within the spindle envelope or in the cytoplasmic region using 405-nm diode-pumped solid state lasers at full power for 30 ms. After bleaching, images were acquired until almost no further recovery was detected. Imaging and bleaching were performed independently by a SIM scanner system.

For data analysis, the following normalization protocol was conducted. First, average fluorescence intensities within the bleached region (I^B), the extracellular region (background, [I_{back}]), and non-bleached cytoplasmic regions (control for bleaching caused by imaging itself, [$I_{cyto}{}^{nB}$]) were measured using the Olympus FV10-ASW software (Olympus). Second, for each frame, the average fluorescence intensity of the bleached region (I^B) and of the non-bleached control cytoplasmic region ($I_{cyto}{}^{nB}$) were normalized by subtracting the intensity of background (outside the embryo region [I_{back}]) in the image. The relative intensities (rI) were calculated as $rI = (I^B - I_{back})/(I_{cyto}{}^{nB} - I_{back})$. The relative intensities were further normalized to the average relative intensities of the 40 frames before bleaching (rI_{pre_ave}) to obtain the normalized intensity (nI), calculated as $nI = rI/rI_{pre\_ave}$. The normalized intensities were plotted against elapsed time after photobleaching, after averaging the intensities obtained in several experiments (normal embryos: bleached nascent spindle region [n = 5] and bleached cytoplasmic region [n = 6]; *ran-1* (RNAi) embryos: bleached nuclear region [n = 5] and bleached cytoplasmic region [n = 7]).

To evaluate the results quantitatively, we fit the plotted data to smooth curves with a least-square fitting algorithm using the Origin Pro software (version 8.5; Origin Lab, Northampton, MA). In FRAP experiments, a simple recovery can be fitted to an exponential curve with a single component. In our analyses, because exponential curves with a single component did not fit well with the data, we fitted the data to exponential curves with two components. The fitted curve can be represented by the following equation:

$$F(t) = A_1 \times [1 - B \times \exp(-t/\tau_1) - (1 - B) \times \exp(-t/\tau_2)] + A_0 \quad (1)$$

where F(t) is the normalized fluorescence intensity at a time t; A_0 is the normalized intensity immediately after photobleaching; A_1 is the increase in the normalized intensity at saturation (>15 s) after the photobleaching from A_0; τ_1 and τ_2 represent the time required for the lifetime of fluorescence recovery for the two components ($\tau_1 < \tau_2$); and B is the proportion of the population of β-tubulin:GFP within τ_1, which is a faster mobile population of total amount of the fluorescence recovering in the bleached region. Therefore the slower mobile population was calculated by (1 − B).

For estimation of the immobile fraction (A_∞), the relative intensities were further normalized to set the value obtained just after photobleaching to 0.0 and the value obtained immediately before photobleaching to 1.0. For direct read out of the immobile fraction [%], the normalized FRAP curves were fitted according to the following equation:

$$F(t) = A_\infty \times [1 - B \times \exp(-t/\tau_1) - (1 - B) \times \exp(-t/\tau_2)] \quad (2)$$

where F(t) is the averaged fluorescence intensity at a time t; A_∞ is the immobile fraction [%] in the normalized fluorescence intensity at infinite time (>15 s) after the photobleaching; τ_1, τ_2, and B are as in Eq. 1.; and A_∞, τ_1, τ_2, and B were optimized by best fitting to each FRAP curve.

For the estimation of the proportion of the slower mobile population (1 − *B*), fitting of Eq. 1 to the averaged FRAP curves (without the normalization to A_∞) was conducted. On fitting against all the FRAP curves, the values of τ_1 and τ_2 were fixed to compare the (1 − B) under the same parameter set of τ_1 and τ_2 between all the conditions. To obtain the fixed τ_1 and τ_2, fitting to Eq. 1 was performed using the mixed normalized FRAP data obtained for the nuclear-bleached and cytoplasmic-bleached regions in a normal embryo. The goodness of fit was validated by calculating the residuals from the fit plot (Figure S6).

Bleaching of the entire nascent spindle region

For analysis of the kinetics of tubulin accumulation in the nascent spindle region, the whole spindle region was photobleached after tubulin accumulation in one-cell-stage embryos. Imaging, photobleaching, and image analysis were performed using the Mosaic digital illumination system (Andor Technology) equipped with a spinning-disk confocal system (CSU-X1; Yokogawa) with a 100×/1.40 NA Oil UPlanSApo objective (Olympus) at room temperature. Before bleaching, 20 frames of images were captured at 1-s intervals. Then, the entire nascent spindle region and a cytoplasmic region with a corresponding area size (circular regions with a diameter of 65 pixels, corresponding to ~8.65 μm) were simultaneously photobleached using a 405-nm diode laser at full power for 1 s. After bleaching, 120 frames of images were captured at a 100-ms intervals, followed by 20 frames at 1-s intervals with 50-ms exposures.

For determination of the bleached area along the *z*-axis, embryos fixed and stained with an anti-α-tubulin antibody were bleached using the same conditions as described above in *FRAP*. The fixed embryo was imaged every 0.2 μm over 16 μm in thickness, which corresponds approximately to the depth of the embryo, to obtain Z-stacks. Three-dimensional reconstruction of the confocal sequence along the *z*-axis was created using Volume Viewer from the Image J software (NIH).

Statistical analysis

Statistical differences in Figure 5 were calculated using Student's *t* test in Microsoft Excel (Microsoft). Statistical differences in Figure 6 were evaluated by whether confidence intervals at 95% confidence level of the two groups overlapped or not. The 95% confidence interval was calculated based on SE values calculated by the Origin software (OriginLab).

ACKNOWLEDGMENTS

We thank Anjon Audhya (University of Wisconsin–Madison Medical School), Ian Mattaj and Matatyas Gorjanacz (European Molecular Biology Laboratory [EMBL]), Karen Oegema (University of California), John White and Ahna Skop (University of Wisconsin), Yuji Kohara (National Institute of Genetics [NIG]), and the *Caenorhabditis* Genetic Center for providing strains and reagents. In addition, we thank Yasushi Hiromi, Yuji Kohara, Kazuhiro Maeshima, and Emiko Suzuki (NIG), Masamitsu Sato (University of Tokyo), Ian Mattaj, Matatyas Gorjanacz, and Hideki Yokoyama (EMBL), Takashi Murata (National institute for Basic Science), Tokuko Haraguchi (National Institute of Information and Communications Technology), Yasushi Hiraoka (Osaka University), Shintaro Mikuni (Hokkaido University), and the members of the Cell Architecture Laboratory, in particular Yuki Hara and Ritsuya Niwayama, for valuable discussions and

suggestions. We thank Shigenobu Yonemura (RIKEN) for his support. This study was supported by a grant from the Ministry of Education, Culture, Sports, Science, and Technology of Japan; the Transdisciplinary Research Integration Center of the Research Organization of Information and Systems, Japan; and the Graduate University for Advanced Studies (Sokendai).

REFERENCES

Akoumianaki T, Kardassis D, Polioudaki H, Georgatos SD, Theodoropoulos PA (2009). Nucleocytoplasmic shuttling of soluble tubulin in mammalian cells. J Cell Sci 122, 1111–1118.

Alberts BM, Johnson A, Lewis J, Raff M, Roberts K, Walter P (2008). Molecular Biology of the Cell, 5th ed., New York: Garland Science.

Arai K, Sato M, Tanaka K, Yamamoto M (2010). Nuclear compartmentalization is abolished during fission yeast meiosis. Curr Biol 20, 1913–1918.

Asakawa H, Kojidani T, Mori C, Osakada H, Sato M, Ding DQ, Hiraoka Y, Haraguchi T (2010). Virtual breakdown of the nuclear envelope in fission yeast meiosis. Curr Biol 20, 1919–1925.

Askjaer P, Galy V, Hannak E, Mattaj IW (2002). Ran GTPase cycle and importins alpha and beta are essential for spindle formation and nuclear envelope assembly in living *Caenorhabditis elegans* embryos. Mol Biol Cell 13, 4355–4370.

Audhya A, Desai A, Oegema K (2007). A role for Rab5 in structuring the endoplasmic reticulum. J Cell Biol 178, 43–56.

Axelrod D, Koppel DE, Schlessinger J, Elson E, Webb WW (1976). Mobility measurement by analysis of fluorescence photobleaching recovery kinetics. Biophys J 16, 1055–1069.

Bamba C, Bobinnec Y, Fukuda M, Nishida E (2002). The GTPase Ran regulates chromosome positioning and nuclear envelope assembly in vivo. Curr Biol 12, 503–507.

Beaudouin J, Gerlich D, Daigle N, Eils R, Ellenberg J (2002). Nuclear envelope breakdown proceeds by microtubule-induced tearing of the lamina. Cell 108, 83–96.

Brenner S (1974). The genetics of *Caenorhabditis elegans*. Genetics 77, 71–94.

Carazo-Salas RE, Gruss OJ, Mattaj IW, Karsenti E (2001). Ran-GTP coordinates regulation of microtubule nucleation and dynamics during mitotic-spindle assembly. Nat Cell Biol 3, 228–234.

Carazo-Salas RE, Guarguaglini G, Gruss OJ, Segref A, Karsenti E, Mattaj IW (1999). Generation of GTP-bound Ran by RCC1 is required for chromatin-induced mitotic spindle formation. Nature 400, 178–181.

Civelekoglu-Scholey G, Tao L, Brust-Mascher I, Wollman R, Scholey JM (2010). Prometaphase spindle maintenance by an antagonistic motor-dependent force balance made robust by a disassembling lamin-B envelope. J Cell Biol 188, 49–68.

Cockell MM, Baumer K, Gönczy P (2004). *lis-1* is required for dynein-dependent cell division processes in *C. elegans* embryos. J Cell Sci 117, 4571–4582.

Cohen M, Tzur YB, Neufeld E, Feinstein N, Delannoy MR, Wilson KL, Gruenbaum Y (2002). Transmission electron microscope studies of the nuclear envelope in *Caenorhabditis elegans* embryos. J Struct Biol 140, 232–240.

Cowan CR, Hyman AA (2004). Asymmetric cell division in *C. elegans*: cortical polarity and spindle positioning. Annu Rev Cell Dev Biol 20, 427–453.

Dasso M (1993). RCC1 in the cell cycle: the regulator of chromosome condensation takes on new roles. Trends Biochem Sci 18, 96–101.

De Souza CP, Osmani AH, Hashmi SB, Osmani SA (2004). Partial nuclear pore complex disassembly during closed mitosis in *Aspergillus nidulans*. Curr Biol 14, 1973–1984.

Fire A, Xu S, Montgomery MK, Kostas SA, Driver SE, Mello CC (1998). Potent and specific genetic interference by double-stranded RNA in *Caenorhabditis elegans*. Nature 391, 806–811.

Franz C, Askjaer P, Antonin W, Iglesias CL, Haselmann U, Schelder M, de Marco A, Wilm M, Antony C, Mattaj IW (2005). Nup155 regulates nuclear envelope and nuclear pore complex formation in nematodes and vertebrates. EMBO J 24, 3519–3531.

Galy V, Askjaer P, Franz C, Lopez-Iglesias C, Mattaj IW (2006). MEL-28, a novel nuclear-envelope and kinetochore protein essential for zygotic nuclear-envelope assembly in *C. elegans*. Curr Biol 16, 1748–1756.

Galy V, Mattaj IW, Askjaer P (2003). *Caenorhabditis elegans* nucleoporins Nup93 and Nup205 determine the limit of nuclear pore complex size exclusion in vivo. Mol Biol Cell 14, 5104–5115.

Gönczy P, Pichler S, Kirkham M, Hyman AA (1999). Cytoplasmic dynein is required for distinct aspects of MTOC positioning, including centrosome separation, in the one cell stage *Caenorhabditis elegans* embryo. J Cell Biol 147, 135–150.

Green RA, Audhya A, Pozniakovsky A, Dammermann A, Pemble H, Monen J, Portier N, Hyman A, Desai A, Oegema K (2008). Expression and imaging of fluorescent proteins in the *C. elegans* gonad and early embryo. Methods Cell Biol 85, 179–218.

Gruenbaum Y, Margalit A, Goldman RD, Shumaker DK, Wilson KL (2005). The nuclear lamina comes of age. Nat Rev Mol Cell Biol 6, 21–31.

Gruss OJ, Carazo-Salas RE, Schatz CA, Guarguaglini G, Kast J, Wilm M, Le Bot N, Vernos I, Karsenti E, Mattaj IW (2001). Ran induces spindle assembly by reversing the inhibitory effect of importin α on TPX2 activity. Cell 104, 83–93.

Hachet V, Canard C, Gönczy P (2007). Centrosomes promote timely mitotic entry in *C. elegans* embryos. Dev Cell 12, 531–541.

Harel A, Chan RC, Lachish-Zalait A, Zimmerman E, Elbaum M, Forbes DJ (2003). Importin β negatively regulates nuclear membrane fusion and nuclear pore complex assembly. Mol Biol Cell 14, 4387–4396.

Harel A, Zlotkin E, Nainudel-Epszteyn S, Feinstein N, Fisher PA, Gruenbaum Y (1989). Persistence of major nuclear envelope antigens in an envelope-like structure during mitosis in *Drosophila melanogaster* embryos. J Cell Sci 94, 463–470.

Howard J (2001). Mechanics of Motor Proteins and the Cytoskeleton, Sunderland, MA: Sinauer Associates.

Inoue S (1981). Cell division and the mitotic spindle. J Cell Biol 91, 131s–147s.

Johansen J, Johansen KM (2009). The spindle matrix through the cell cycle in Drosophila. Fly (Austin) 3, 213–220.

Johansen KM, Forer A, Yao C, Girton J, Johansen J (2011). Do nuclear envelope and intranuclear proteins reorganize during mitosis to form an elastic, hydrogel-like spindle matrix. Chromosome Res 19, 345–365.

Kalab P, Heald R (2008). The RanGTP gradient—a GPS for the mitotic spindle. J Cell Sci 121, 1577–1586.

Kalab P, Pralle A, Isacoff EY, Heald R, Weis K (2006). Analysis of a RanGTP-regulated gradient in mitotic somatic cells. Nature 440, 697–701.

Kalab P, Pu RT, Dasso M (1999). The ran GTPase regulates mitotic spindle assembly. Curr Biol 9, 481–484.

Kalab P, Weis K, Heald R (2002). Visualization of a Ran-GTP gradient in interphase and mitotic *Xenopus* egg extracts. Science 295, 2452–2456.

Kimura A, Onami S (2005). Computer simulations and image processing reveal length-dependent pulling force as the primary mechanism for *C. elegans* male pronuclear migration. Dev Cell 8, 765–775.

Kirkham M, Muller-Reichert T, Oegema K, Grill S, Hyman AA (2003). SAS-4 is a *C. elegans* centriolar protein that controls centrosome size. Cell 112, 575–587.

Kiseleva E, Rutherford S, Cotter LM, Allen TD, Goldberg MW (2001). Steps of nuclear pore complex disassembly and reassembly during mitosis in early *Drosophila* embryos. J Cell Sci 114, 3607–3618.

Lee KK, Gruenbaum Y, Spann P, Liu J, Wilson KL (2000). *C. elegans* nuclear envelope proteins emerin, MAN1, lamin, and nucleoporins reveal unique timing of nuclear envelope breakdown during mitosis. Mol Biol Cell 11, 3089–3099.

Lenart P, Rabut G, Daigle N, Hand AR, Terasaki M, Ellenberg J (2003). Nuclear envelope breakdown in starfish oocytes proceeds by partial NPC disassembly followed by a rapidly spreading fenestration of nuclear membranes. J Cell Biol 160, 1055–1068.

Lince-Faria M, Maffini S, Orr B, Ding Y, Claudia F, Sunkel CE, Tavares A, Johansen J, Johansen KM, Maiato H (2009). Spatiotemporal control of mitosis by the conserved spindle matrix protein Megator. J Cell Biol 184, 647–657.

Liu J, Rolef Ben-Shahar T, Riemer D, Treinin M, Spann P, Weber K, Fire A, Gruenbaum Y (2000). Essential roles for *Caenorhabditis elegans* lamin gene in nuclear organization, cell cycle progression, and spatial organization of nuclear pore complexes. Mol Biol Cell 11, 3937–3947.

Meyerzon M, Gao Z, Liu J, Wu JC, Malone CJ, Starr DA (2009). Centrosome attachment to the *C. elegans* male pronucleus is dependent on the surface area of the nuclear envelope. Dev Biol 327, 433–446.

Nachury MV, Maresca TJ, Salmon WC, Waterman-Storer CM, Heald R, Weis K (2001). Importin β is a mitotic target of the small GTPase Ran in spindle assembly. Cell 104, 95–106.

Ohba T, Nakamura M, Nishitani H, Nishimoto T (1999). Self-organization of microtubule asters induced in *Xenopus* egg extracts by GTP-bound Ran. Science 284, 1356–1358.

Ohno M, Fornerod M, Mattaj IW (1998). Nucleocytoplasmic transport: the last 200 nanometers. Cell 92, 327–336.

Ookata K, Hisanaga S, Okano T, Tachibana K, Kishimoto T (1992). Relocation and distinct subcellular localization of p34cdc2-cyclin B complex at meiosis reinitiation in starfish oocytes. EMBO J 11, 1763–1772.
Ovechkina Y, Maddox P, Oakley CE, Xiang X, Osmani SA, Salmon ED, Oakley BR (2003). Spindle formation in *Aspergillus* is coupled to tubulin movement into the nucleus. Mol Biol Cell 14, 2192–2200.
Pines J, Hunter T (1991). Human cell division: the involvement of cyclins A and B1, and multiple cdc2s. Cold Spring Harb Symp Quant Biol 56, 449–463.
Poirier CC, Zheng Y, Iglesias PA (2010). Mitotic membrane helps to focus and stabilize the mitotic spindle. Biophys J 99, 3182–3190.
Portier N, Audhya A, Maddox PS, Green RA, Dammermann A, Desai A, Oegema K (2007). A microtubule-independent role for centrosomes and Aurora A in nuclear envelope breakdown. Dev Cell 12, 515–529.
Qi H *et al*. (2004). Megator, an essential coiled-coil protein that localizes to the putative spindle matrix during mitosis in *Drosophila*. Mol Biol Cell 15, 4854–4865.
Rump A, Scholz T, Thiel C, Hartmann FK, Uta P, Hinrichs MH, Taft MH, Tsiavaliaris G (2011). Myosin-1C associates with microtubules and stabilizes the mitotic spindle during cell division. J Cell Sci 124, 2521–2528.
Salina D, Bodoor K, Eckley DM, Schroer TA, Rattner JB, Burke B (2002). Cytoplasmic dynein as a facilitator of nuclear envelope breakdown. Cell 108, 97–107.
Salus SS, Demeter J, Sazer S (2002). The Ran GTPase system in fission yeast affects microtubules and cytokinesis in cells that are competent for nucleocytoplasmic protein transport. Mol Cell Biol 22, 8491–8505.
Sato M, Okada N, Kakui Y, Yamamoto M, Yoshida M, Toda T (2009). Nucleocytoplasmic transport of Alp7/TACC organizes spatiotemporal microtubule formation in fission yeast. EMBO Rep 10, 1161–1167.
Sato M, Toda T (2007). Alp7/TACC is a crucial target in Ran-GTPase-dependent spindle formation in fission yeast. Nature 447, 334–337.
Schwarzerova K, Petrasek J, Panigrahi KC, Zelenkova S, Opatrny Z, Nick P (2006). Intranuclear accumulation of plant tubulin in response to low temperature. Protoplasma 227, 185–196.
Skop AR, White JG (1998). The dynactin complex is required for cleavage plane specification in early *Caenorhabditis elegans* embryos. Curr Biol 8, 1110–1116.
Sprague BL, Pego RL, Stavreva DA, McNally JG (2004). Analysis of binding reactions by fluorescence recovery after photobleaching. Biophys J 86, 3473–3495.
Srayko M, Kaya A, Stamford J, Hyman AA (2005). Identification and characterization of factors required for microtubule growth and nucleation in the early *C. elegans* embryo. Dev Cell 9, 223–236.
Stafstrom JP, Staehelin LA (1984). Dynamics of the nuclear envelope and of nuclear pore complexes during mitosis in the Drosophila embryo. Eur J Cell Biol 34, 179–189.
Straube A, Brill M, Oakley BR, Horio T, Steinberg G (2003). Microtubule organization requires cell cycle-dependent nucleation at dispersed cytoplasmic sites: polar and perinuclear microtubule organizing centers in the plant pathogen *Ustilago maydis*. Mol Biol Cell 14, 642–657.
Straube A, Weber I, Steinberg G (2005). A novel mechanism of nuclear envelope break-down in a fungus: nuclear migration strips off the envelope. EMBO J 24, 1674–1685.
Strome S, Wood WB (1983). Generation of asymmetry and segregation of germ-line granules in early *C. elegans* embryos. Cell 35, 15–25.
Terasaki M, Campagnola P, Rolls MM, Stein PA, Ellenberg J, Hinkle B, Slepchenko B (2001). A new model for nuclear envelope breakdown. Mol Biol Cell 12, 503–510.
Terasawa M, Toya M, Motegi F, Mana M, Nakamura K, Sugimoto A (2010). *Caenorhabditis elegans* ortholog of the p24/p22 subunit, DNC-3, is essential for the formation of the dynactin complex by bridging DNC-1/p150(Glued) and DNC-2/dynamitin. Genes Cells 15, 1145–1157.
Toya M, Terasawa M, Nagata K, Iida Y, Sugimoto A (2011). A kinase-independent role for Aurora A in the assembly of mitotic spindle microtubules in *Caenorhabditis elegans* embryos. Nat Cell Biol 13, 708–714.
Tsai MY, Wang S, Heidinger JM, Shumaker DK, Adam SA, Goldman RD, Zheng Y (2006). A mitotic lamin B matrix induced by RanGTP required for spindle assembly. Science 311, 1887–1893.
Ukil L, De Souza CP, Liu HL, Osmani SA (2009). Nucleolar separation from chromosomes during *Aspergillus nidulans* mitosis can occur without spindle forces. Mol Biol Cell 20, 2132–2145.
Walker DL, Wang D, Jin Y, Rath U, Wang Y, Johansen J, Johansen KM (2000). Skeletor, a novel chromosomal protein that redistributes during mitosis provides evidence for the formation of a spindle matrix. J Cell Biol 151, 1401–1412.
Wiese C, Wilde A, Moore MS, Adam SA, Merdes A, Zheng Y (2001). Role of importin-β in coupling Ran to downstream targets in microtubule assembly. Science 291, 653–656.
Wilde A, Lizarraga SB, Zhang L, Wiese C, Gliksman NR, Walczak CE, Zheng Y (2001). Ran stimulates spindle assembly by altering microtubule dynamics and the balance of motor activities. Nat Cell Biol 3, 221–227.
Wilde A, Zheng Y (1999). Stimulation of microtubule aster formation and spindle assembly by the small GTPase Ran. Science 284, 1359–1362.
Wittmann T, Hyman A, Desai A (2001). The spindle: a dynamic assembly of microtubules and motors. Nat Cell Biol 3, E28–E34.
Zheng Y (2010). A membranous spindle matrix orchestrates cell division. Nat Rev Mol Cell Biol 11, 529–535.